Journal of Sound and Vibration (2001) **246**(3), 389–402
doi:10.1006/jsvi.2001.3673, available online at http://www.idealibrary.com on IDEAL®

DYNAMIC ANALYSIS OF FLEXIBLE SLIDER-CRANK MECHANISMS WITH NON-LINEAR FINITE ELEMENT METHOD

J.-S. Chen and C.-L. Huang

Department of Mechanical Engineering, National Taiwan University, Taipei, Taiwan 10617, *Republic of China. E-mail: jschen@w3.me.ntu.edu.tw*

(*Received* 6 *June* 2000, *and in final form* 13 *November* 2000)

Previous research in finite element formulation of flexible mechanisms usually neglected high order terms in the strain-energy function. In particular, the quartic term of the displacement gradient is always neglected due to the common belief that it is not important in the dynamic analysis. In this paper, we show that this physical intuition is not always valid. By retaining all the high order terms in the strain-energy function the equations of motion naturally become non-linear, which can then be solved by the Newmark method. In the low-speed range it is found that the dynamic responses predicted by non-linear and linear approaches indeed make no significant difference. However, when the rotation speed increases up to about one-fifth of the fundamental bending natural frequency of the connecting rod, simplified approaches begin to incur noticeable error. Specifically, for a connecting rod with a slenderness ratio of 0·01 the conventional simplified approaches overestimate the vibration amplitude almost 10-fold when the rotation speed is comparable to the fundamental natural frequency of the connecting rod. Therefore, non-linear finite element formulation taking into account the complete non-linear strain is needed in analyzing high-speed flexible mechnisms with slender links.

1. INTRODUCTION AND STRAIN ENERGY

Finite element methods have been widely used in analyzing the dynamic response of flexible mechanisms and robotic manipulators. Some comprehensive surveys can be found in Erdman and Sandor [1], Lowen and Jandrasits [2], and Thompson and Sung [3]. The formulation procedure consists of deriving kinetic energy and strain energy of each element, using shape functions to approximate the displacement field, applying Hamilton's principle to obtain the discretized equations of motion of the element, and finally assembling the elements appropriately to obtain the global equations of motion. Beam elements are commonly used in modelling the members of linkages.

Among numerous types of linkages, slider-crank mechanism may be the simplest and most commonly used in practice. Figure 1 shows a typical slider-crank mechanism with rigid crank a and flexible connecting rod L. The rigid crank rotates with constant speed Ω. The cross-sectional area, mass density, and Young's modulus of the elastic connecting rod are A, ρ, and E respectively. XOY is an inertial frame with its origin attached to the center of the rotating crank. xAy is a moving frame with x-axis passing through the two ends of the connecting rod before deformation. $u(x, t)$ and $v(x, t)$ denote the axial and transverse displacements of the neutral axis of the connecting rod. When the mechanism is in

0022-460X/01/380389 + 14 $35.00/0

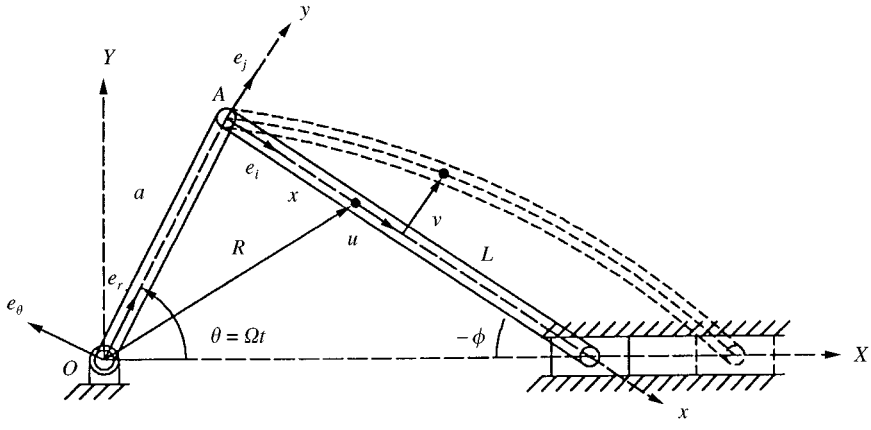

Figure 1. Schematic diagram of a slider-crank mechanism.

operation the connecting rod is in general subject to both axial and transverse forces. As a consequence, the displacements u and v are coupled.

To correctly model the coupling between axial vibration and transverse deflection in analysis, non-linear strain measure has to be used in deriving the strain energy. For instance, if the Euler–Bernoulli beam model is adopted, the axial strain of a point (x, y) in the connecting rod can be written as

$$e_{xx} = u_{,x} + \tfrac{1}{2} v_{,x}^2 - y v_{,xx}. \tag{1}$$

Following a volume integral, the strain energy U_c of the connecting rod can be written as

$$U_c = \frac{1}{2} \int_0^L \left[EA\left(u_{,x}^2 + u_{,x} v_{,x}^2 + \frac{1}{4} v_{,x}^4 \right) + EI v_{,xx}^2 \right] \mathrm{d}x. \tag{2}$$

Different approaches have been adopted in the literature to simplify equation (2). First of all, if linear strain (neglecting $\frac{1}{2} v_{,x}^2$ in equation (1)) is used, there will be no coupling between axial and transverse vibrations. This simple approach has been adopted by Bahgat and Willmert [4], Midha *et al.* [5], Sunada and Dubowsky [6], Yang and Sadler [7], and Fung and Chen [8].

The second approach is to use the non-linear strain as given in equation (1), but ignore the quartic term $\frac{1}{4} v_{,x}^4$ in equation (2). Furthermore, the axial force $P(x)$ is used to replace $EAu_{,x}$, and equation (2) is rewritten as

$$U_c = \frac{1}{2} \int_0^L [EAu_{,x}^2 + EIv_{,xx}^2 + P(x)v_{,x}^2] \, \mathrm{d}x. \tag{3}$$

The strain energy is then a function of quadratic terms of displacement gradients, and the resulting equations of motion are linear in terms of u and v. In this formulation, the axial displacement will not be affected by the transverse deflection and can be calculated first. The transverse deflection will then be influenced by the axial vibration. This is a popular approach in many finite element textbooks, and in the flexible mechanism research community as well, for instance, see Nath and Ghosh [9], Cleghorn *et al.* [10], Turcic and Midha [11], and Thompson and Sung [12]. Sometimes it is called a geometrically non-linear approach [3].

It is commonly believed that the quartic term $\frac{1}{4}v_{,x}^4$ is not important in the dynamic analysis of flexible slider-crank mechanism. However, whether this intuition is valid or not has never been examined before. In the present formulation, we retain all the high order terms in the strain-energy function. The equations of motion become non-linear in terms of the transverse deflection v. If the equations are put in the conventional matrix form the stiffness matrix will contain unknown v, and an iterative method is required to calculate the response. In this paper, the Newmark method is used for integration. Crank rotation speed and slenderness ratio of the connecting rod are two important parameters whose effects on the accuracy of various approaches will be examined closely. It is found that the conventional impression regarding the negligibility of the quartic term is not valid. In particular, neglecting the quartic term results in considerable error for links with small slenderness ratio when the crank speed is over one-fifth the fundamental natural frequency of the connecting rod. The effect of slider mass on the extension of the connecting rod is also studied in detail.

2. KINETIC ENERGY

Referring back to Figure 1 the position vector $\mathbf{R}$ of a point in the connecting rod measured from the pivot O can be written as

$$\mathbf{R} = a\mathbf{e}_r + (x + u - yv_{,x})\mathbf{e}_i + (y + v)\mathbf{e}_j, \tag{4}$$

where $(\mathbf{e}_r, \mathbf{e}_\theta)$ and $(\mathbf{e}_i, \mathbf{e}_j)$ are rotating base vectors attached to points O and A respectively. The kinetic energy T_c of the connecting rod is

$$T_c = \frac{1}{2}\int_V \rho\dot{\mathbf{R}}\cdot\dot{\mathbf{R}}\,\mathrm{d}V. \tag{5}$$

The kinetic energy of the slider T_s is

$$T_s = \frac{m_s}{2}\dot{\mathbf{R}}_s\cdot\dot{\mathbf{R}}_s, \tag{6}$$

where m_s and $\dot{\mathbf{R}}_s$ are the mass and velocity of the slider,

$$\dot{\mathbf{R}}_s = [-a\dot{\theta}\sin(\theta + \phi) + u_{,t} + v\dot{\phi}]\mathbf{e}_i + [a\dot{\theta}\cos(\theta + \phi) - (L + u)\dot{\phi} + v_{,t}]\mathbf{e}_j, \tag{7}$$

where ϕ is the angle between the x-axis and X-axis, and θ is the rotation angle of the crank. The kinetic energy of the rigid crank will not enter the equations of motion and is ignored in the formulation.

3. FINITE ELEMENT FORMULATION

We divide the connecting rod into n elements of equal length $l = L/n$. The two nodes of the ith element are nodes i and $i + 1$ respectively. Within this element we assume that the displacements u, v, and slope ψ of the neutral axis can be interpolated in the following manner:

$$u = \{\mathbf{N}_u\}^{\mathrm{T}}\{\mathbf{q}\}_i, \tag{8}$$

$$v = \{\mathbf{N}_v\}^{\mathrm{T}}\{\mathbf{q}\}_i, \tag{9}$$

$$\psi = \{\mathbf{N}_\psi\}^{\mathrm{T}}\{\mathbf{q}\}_i, \tag{10}$$

where shape function vectors $\{\mathbf{N}_u\}$, $\{\mathbf{N}_v\}$, $\{\mathbf{N}_\psi\}$, and nodal vector $\{\mathbf{q}\}_i$ are defined as

$$\{\mathbf{N}_u\} = \{N_{u1}, 0, 0, N_{u2}, 0, 0\}^{\mathrm{T}}, \tag{11}$$

$$\{\mathbf{N}_v\} = \{0, N_{v1}, N_{v2}, 0, N_{v3}, N_{v4}\}^{\mathrm{T}}, \tag{12}$$

$$\{\mathbf{N}_\psi\} = \{0, N_{\psi 1}, N_{\psi 2}, 0, N_{\psi 3}, N_{\psi 4}\}^{\mathrm{T}}, \tag{13}$$

$$\{\mathbf{q}\}_i = \{u_i, v_i, \psi_i, u_{i+1}, v_{i+1}, \psi_{i+1}\}^{\mathrm{T}}. \tag{14}$$

$\{\mathbf{N}_u\}$, $\{\mathbf{N}_v\}$, $\{\mathbf{N}_\psi\}$ are linear, cubic, and quadratic functions of x, respectively, and are detailed in Appendix A. In terms of the nodal vector the kinetic energy and strain energy of the connecting rod can be expressed as

$$T_c = \sum_{i=1}^{n} T_i, \tag{15}$$

$$U_c = \sum_{i=1}^{n} U_i, \tag{16}$$

where the kinetic energy and strain energy in element i are

$$T_i = \tfrac{1}{2}\{\dot{\mathbf{q}}\}_i^{\mathrm{T}}[\mathbf{m}_1]\{\dot{\mathbf{q}}\}_i + \tfrac{1}{2}\{\mathbf{q}\}_i^{\mathrm{T}}[\mathbf{m}_2]\{\mathbf{q}\}_i + \{\dot{\mathbf{q}}\}_i^{\mathrm{T}}\{\mathbf{m}_3\} + \{\mathbf{q}\}_i^{\mathrm{T}}\{\mathbf{m}_4\}, \tag{17}$$

$$U_i = \tfrac{1}{2}\{\mathbf{q}\}_i^{\mathrm{T}}([\mathbf{k}_{uu}] + [\mathbf{k}_{\psi\psi}] + [\mathbf{k}_{Pvv}])\{\mathbf{q}\}_i + \tfrac{1}{2}\{\mathbf{q}\}_i^{\mathrm{T}}[\mathbf{k}_{vvvv}]\{\mathbf{q}\}_i. \tag{18}$$

The associated matrices and vectors are given in Appendix B. By applying Hamilton's principle

$$\int_{t_1}^{t_2} (\delta T_c + \delta T_s - \delta U_c)\,\mathrm{d}t = 0, \tag{19}$$

we can obtain the equation of motion of the ith element as

$$[\mathbf{m}]\{\ddot{\mathbf{q}}\}_i + [\mathbf{c}]\{\dot{\mathbf{q}}\}_i + ([\mathbf{k}_{lin}] + [\mathbf{k}_{non}(\{\mathbf{q}\}_i)])\{\mathbf{q}\}_i = \{\mathbf{f}\}, \tag{20}$$

where

$$[\mathbf{m}] = [\mathbf{m}_1], \tag{21}$$

$$[\mathbf{k}_{lin}] = [\mathbf{k}_{uu}] + \lfloor \mathbf{k}_{\psi\psi} \rfloor + [\mathbf{k}_{Pvv}] - [\mathbf{m}_2], \tag{22}$$

$$[\mathbf{k}_{non}] = 2[\mathbf{k}_{vvvv}], \tag{23}$$

$$[\mathbf{c}] = \mu([\mathbf{k}_{lin}] + [\mathbf{k}_{non}]), \tag{24}$$

$$\{\mathbf{f}\} = \{\mathbf{m}_4\} - \{\dot{\mathbf{m}}_3\}. \tag{25}$$

It is noted that in equation (24) we assume that damping is proportional to the stiffness matrix. For the nth element which is attached to the slider, the displacements u_{n+1} and v_{n+1} are constrained in the following manner [8]:

$$v_{n+1} = u_{n+1} \tan\phi. \tag{26}$$

As a consequence, some of the matrices in equation (20) for the nth element are modified as

$$[\mathbf{m}] = [\mathbf{m}_1] + [\mathbf{m}_{s1}], \tag{27}$$

$$[\mathbf{k}_{lin}] = [\mathbf{k}_{uu}] + [\mathbf{k}_{\psi\psi}] + [\mathbf{k}_{Pvv}] - [\mathbf{m}_2] - [\mathbf{m}_{s2}], \tag{28}$$

$$\{\mathbf{f}\} = \{\mathbf{m}_4\} - \{\dot{\mathbf{m}}_3\} + \{\mathbf{m}_{s3}\} - \{\mathbf{m}_{s4}\}. \tag{29}$$

Matrices $[\mathbf{m}_{s1}]$, $[\mathbf{m}_{s2}]$, and vectors $\{\mathbf{m}_{s3}\}$, $\{\mathbf{m}_{s4}\}$ are given in Appendix B.

The above formulation taking into account the high order term in the strain-energy function is called approach (A) in this paper. If the quartic term $\frac{1}{4} v_{,x}^4$ is neglected in equation (1), then the matrix $[\mathbf{k}_{vvvv}]$ will disappear in equation (20). We call this approach (B). Furthermore, if linear strain is assumed in equation (1), the term $[\mathbf{k}_{Pvv}]$ (sometimes called geometric stiffness matrix in the literature [11]) in equations (22) and (28) will also disappear. We call this approach (C).

After deriving the equation of motion (20) for each element, we can assemble the elements by enforcing compatibility on the displacements and slopes at each node. It is noted that in assembling the global equations we treat the unknowns in matrix $[\mathbf{k}_{non}]$ as known constants. Finally, the global equations of motion are obtained in the form

$$[\mathbf{M}]\{\ddot{\mathbf{Q}}\} + [\mathbf{C}]\{\dot{\mathbf{Q}}\} + ([\mathbf{K}_{lin}] + [\mathbf{K}_{non}(\{\mathbf{Q}\})])\{\mathbf{Q}\} = \{\mathbf{F}\}, \tag{30}$$

where $\{\mathbf{Q}\}$ is the global nodal vector.

4. NEWMARK METHOD

The Newmark method [13] is particularly useful in integrating non-linear equation (30). We denote the acceleration, velocity, and displacement at time t_m as

$$\{\hat{\mathbf{a}}\}_m = \{\ddot{\mathbf{Q}}\}_m, \tag{31}$$

$$\{\hat{\mathbf{v}}\}_m = \{\dot{\mathbf{Q}}\}_m, \tag{32}$$

$$\{\hat{\mathbf{d}}\}_m = \{\mathbf{Q}\}_m. \tag{33}$$

Given $\{\hat{\mathbf{d}}\}_m$ and $\{\hat{\mathbf{v}}\}_m$ ($m = 0$ for initial conditions), we can solve $\{\mathbf{a}\}_m$ from

$$[\mathbf{M}]\{\hat{\mathbf{a}}\}_m = \{\mathbf{F}\} - [\mathbf{C}]\{\hat{\mathbf{v}}\}_m - ([\mathbf{K}_{lin}] + [\mathbf{K}_{non}(\{\hat{\mathbf{d}}\}_m)])\{\hat{\mathbf{d}}\}_m. \tag{34}$$

The Newmark method calls for the calculation of two predictors $\{\tilde{\mathbf{d}}\}_{m+1}$ and $\{\tilde{\mathbf{v}}\}_{m+1}$,

$$\{\tilde{\mathbf{d}}\}_{m+1} = \{\hat{\mathbf{d}}\}_m + \Delta t\{\hat{\mathbf{v}}\}_m + \frac{\Delta t^2}{2}(1 - 2\beta)\{\hat{\mathbf{a}}\}_m, \tag{35}$$

$$\{\tilde{\mathbf{v}}\}_{m+1} = \{\hat{\mathbf{v}}\}_m + \Delta t(1 - \gamma)\{\hat{\mathbf{a}}\}_m, \tag{36}$$

where Δt is the time increment, and β and γ are two constants. In this paper, we choose $\beta = 0{\cdot}25$ and $\gamma = 0{\cdot}5$. After obtaining the predictors we can calculate $\{\hat{\mathbf{a}}\}_{m+1}$ from

$$\begin{aligned}([\mathbf{M}] + \gamma\Delta t[\mathbf{C}] + \beta\Delta t^2([\mathbf{K}_{lin}] + [\mathbf{K}_{non}(\{\tilde{\mathbf{d}}\}_{m+1})]))\{\hat{\mathbf{a}}\}_{m+1} \\ = \{\mathbf{F}\}_{m+1} - [\mathbf{C}]\{\tilde{\mathbf{v}}\}_{m+1} - ([\mathbf{K}_{lin}] + [\mathbf{K}_{non}(\{\tilde{\mathbf{d}}\}_{m+1})])\{\tilde{\mathbf{d}}\}_{m+1}.\end{aligned} \tag{37}$$

Finally $\{\hat{\mathbf{d}}\}_{m+1}$ and $\{\hat{\mathbf{v}}\}_{m+1}$ can be obtained from

$$\{\hat{\mathbf{d}}\}_{m+1} = \{\tilde{\mathbf{d}}\}_{m+1} + \beta \Delta t^2 \{\hat{\mathbf{a}}\}_{m+1}, \tag{38}$$

$$\{\mathbf{v}\}_{m+1} = \{\tilde{\mathbf{v}}\}_m + \gamma \Delta t \{\hat{\mathbf{a}}\}_{m+1}. \tag{39}$$

5. CONVERGENCE TEST

In presenting the calculation results the following dimensionless parameters (with asterisk) are used:

$$a^* = \frac{a}{L}, \quad u^* = \frac{Lu}{r^2}, \quad v^* = \frac{v}{r}, \quad x^* = \frac{x}{L}, \quad \varepsilon = \frac{r}{L}, \quad m_s^* = \frac{m_s}{\rho A L},$$

$$\Omega^* = \frac{\Omega}{\omega_b}, \quad t^* = \omega_b t, \quad \mu^* = \omega_b \mu,$$

where ω_b is the lowest bending natural frequency of the connecting rod,

$$\omega_b = \frac{\pi^2}{L^2}\sqrt{\frac{EI}{\rho A}}.$$

r is the radius of gyration of the cross-section and ε is the slenderness ratio of the connecting rod. We first study the low-speed case $\Omega^* = 0{\cdot}1$. Figure 2 shows the transverse deflection v^* at the middle point of the connecting rod with zero initial conditions. The results from approaches (A), (B), and (C) are presented for comparison. The parameters used in Figure 2 are $a^* = 0{\cdot}1$, $\varepsilon = 0{\cdot}01$, $m_s^* = 0{\cdot}5$, and $\mu^* = 0{\cdot}5$. The time increment Δt^* is set to be equal to

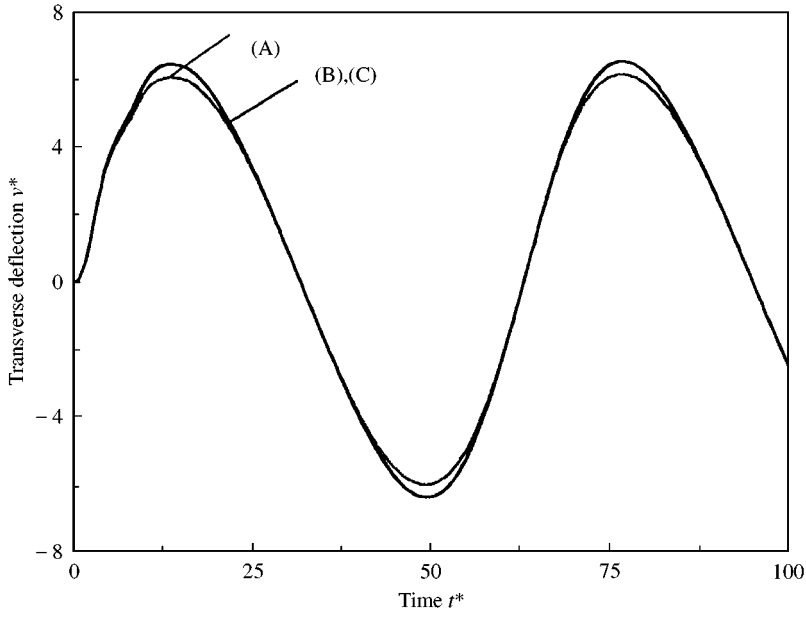

Figure 2. Transverse deflection v^* at $\Omega^* = 0{\cdot}1$ from three different approaches. Four elements are used in all three approaches. $a^* = 0{\cdot}1$, $\varepsilon = 0{\cdot}01$, $m_s^* = 0{\cdot}5$, and $\mu^* = 0{\cdot}5$.

one-hundredth of the period of the crank rotation. The results from two and four elements are almost indistinguishable in all three approaches. Furthermore, the effects of neglecting the quartic term or using linear strain are almost negligible in the low-speed case.

Figure 3 shows the results of the high-speed case $\Omega^* = 0{\cdot}8$ obtained by approach (A) with different numbers of elements used. It is observed that 16 elements are needed to achieve

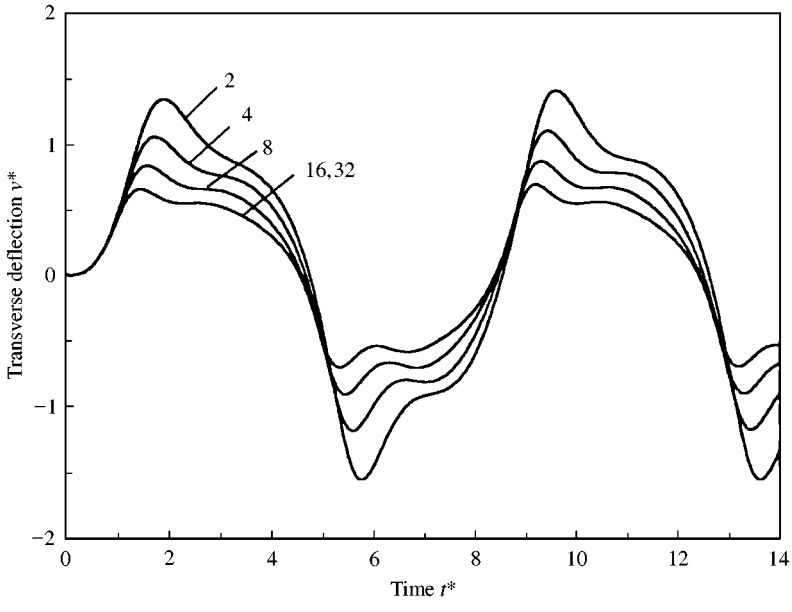

Figure 3. Convergence test for complete non-linear strain approach (A) at high speed $\Omega^* = 0{\cdot}8$. 16 elements are needed to achieve satisfactory convergence. $a^* = 0{\cdot}1$, $\varepsilon = 0{\cdot}01$, $m_s^* = 0{\cdot}5$, and $\mu^* = 0{\cdot}5$.

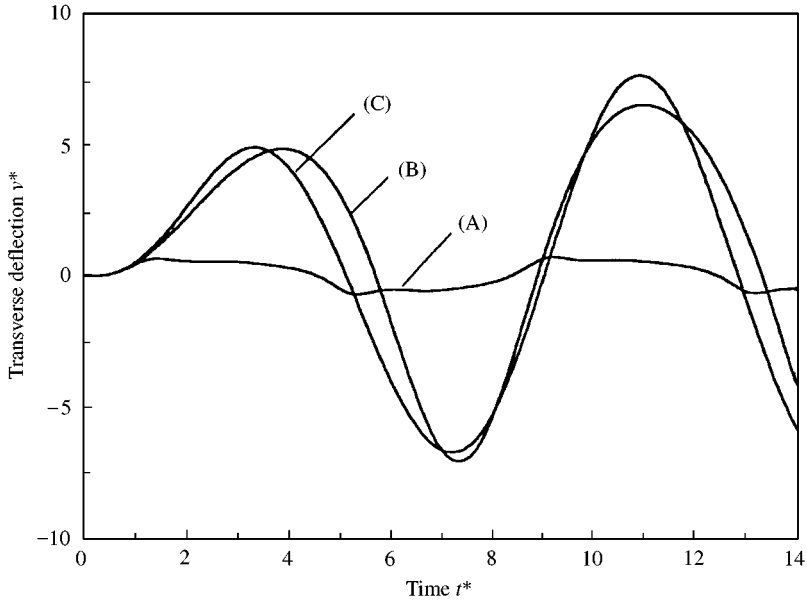

Figure 4. Comparison of transient responses at high speed $\Omega^* = 0{\cdot}8$ from approaches (A), (B), and (C). $a^* = 0{\cdot}1$, $\varepsilon = 0{\cdot}01$, $m_s^* = 0{\cdot}5$, and $\mu^* = 0{\cdot}5$.

satisfactory convergence. For 16-element division, the results from dividing the crank rotation period into 100 and 200 intervals make no difference. On the other hand, for approaches (B) and (C), four elements are again sufficient for satisfactory convergence even in the high-speed case.

In Figure 4 we compare the transient responses calculated by approaches (A), (B), and (C). Four elements are used in approaches (B) and (C), and 16 elements are used in (A). First of all, the effect of neglecting $[\mathbf{k}_{Pvv}]$ (approach (C)) becomes noticeable compared to the result from approach (B), especially when the slider mass is increased. Actually for approach (C) the slider mass has no effect on the transverse deflection because axial force has no influence on the transverse vibration. More importantly, the amplitude of the response from complete non-linear strain approach (A) is about one-tenth of those predicted by approaches (B) and (C). In other words, neglecting the quartic term may be inadequate in predicting the dynamic response of flexible mechanisms at high speed. In the following section, we continue to examine the effects of the quartic term on the steady state response. In each study, 16 elements are used for approach (A), and 4 elements are used for approaches (B) and (C).

6. STEADY STATE RESPONSE

6.1. SLENDERNESS RATIO

Figure 5 shows the steady state amplitude at the middle point of the connecting rod as a function of slenderness ratio ε. The parameters chosen are $a^* = 0{\cdot}1$, $m_s^* = 0{\cdot}5$, and $\mu^* = 0{\cdot}5$. The results from $\Omega^* = 0{\cdot}1$ (dashed lines) and $\Omega^* = 0{\cdot}8$ (solid lines) are plotted in the same figure for comparison. For low speed $\Omega^* = 0{\cdot}1$, the three different approaches produce almost the same result. For high speed $\Omega^* = 0{\cdot}8$, on the other hand, neglecting the

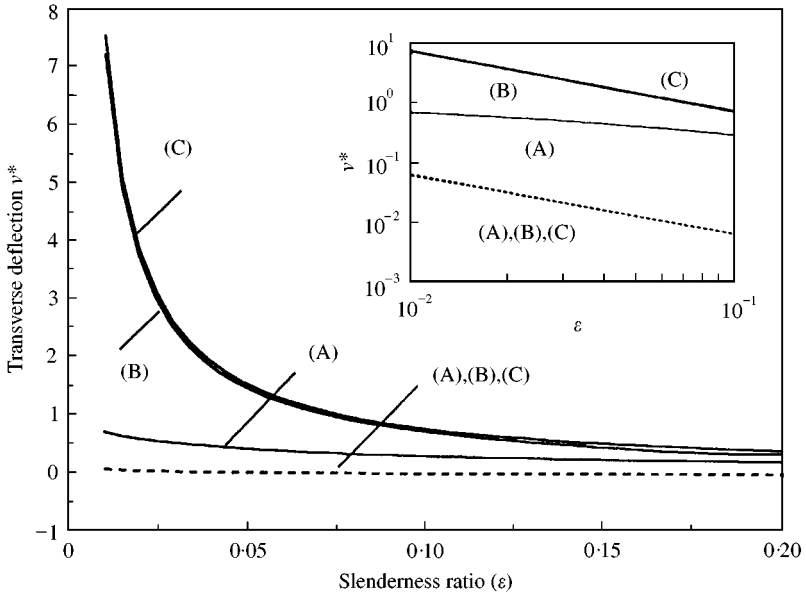

Figure 5. Steady state amplitude v^* as a function of slenderness ratio ε for $\Omega^* = 0{\cdot}1$ (dashed lines) and $\Omega^* = 0{\cdot}8$ (solid lines). $a^* = 0{\cdot}1$, $m_s^* = 0{\cdot}5$, and $\mu^* = 0{\cdot}5$. The inset shows the almost linear relations between log v^* and log ε.

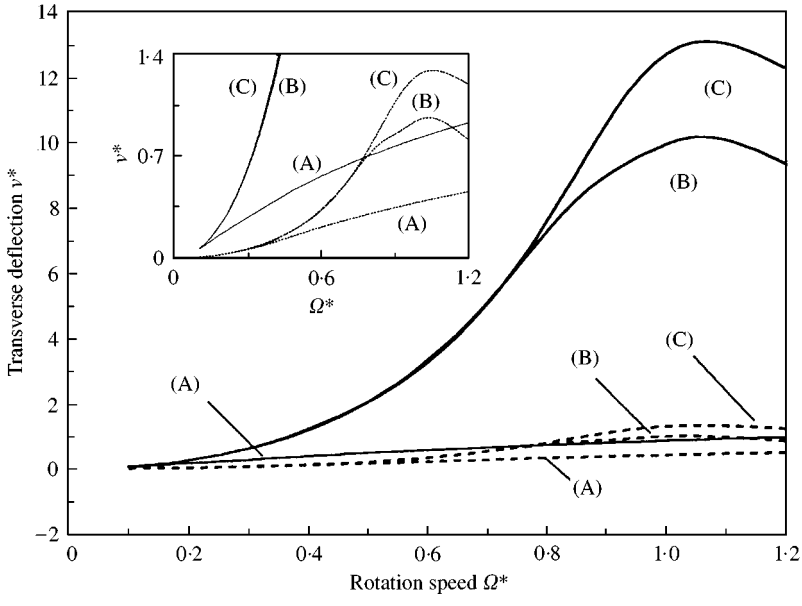

Figure 6. Steady state amplitude v^* as a function of Ω^* for $\varepsilon = 0{\cdot}01$. (solid lines) and $\varepsilon = 0{\cdot}1$ (dashed lines). $a^* = 0{\cdot}1$, $m_s^* = 0{\cdot}5$, and $\mu^* = 0{\cdot}5$. The inset magnifies the range of v^* from 0 to 1·4.

quartic term will overestimate the response about 10-fold when $\varepsilon = 0{\cdot}01$. The differences from approaches (B) and (C) are negligible even in the high-speed range. In all cases the amplitude is almost inversely proportional to ε. This can be observed from the inset of Figure 5, which shows the almost linear relations between $\log v^*$ and $\log \varepsilon$.

6.2. ROTATION SPEED

Figure 6 shows the effect of rotation speed Ω^* on the steady state deflection v^* for two slenderness ratios $\varepsilon = 0{\cdot}01$ (solid lines) and 0·1 (dashed lines). For $\varepsilon = 0{\cdot}01$, approaches (B) and (C) produce almost the same results when $\Omega^* < 0{\cdot}7$. However, they are good approximations to the solution from approach (A) only when $\Omega^* < 0{\cdot}2$. In particular, approaches (B) and (C) overestimate the amplitude 10-fold compared to the one predicted by (A) when $\Omega^* = 1$. Furthermore, while approaches (B) and (C) predict a maximum of amplitude around $\Omega^* = 1$, approach (A) predicts that the amplitude continues to grow as Ω^* increases beyond 1. The inset of Figure 6 magnifies the range of v^* from 0 to 1·4. The relations between the results from approaches (A), (B), and (C) for $\varepsilon = 0{\cdot}1$ are similar to those for $\varepsilon = 0{\cdot}01$, except that the amplitude are about one-tenth of the small slenderness case. For $\varepsilon = 0{\cdot}1$, approaches (B) and (C) approximate approach (A) well when $\Omega^* < 0{\cdot}4$.

6.3. SLIDER MASS

In Figure 7 we show the effect of slider mass on the steady state extension of the connecting rod during a crank rotation period at high speed $\Omega^* = 0{\cdot}8$. Approach (A) is adopted for four different values of m_s^*, i.e., 0, 0·5, 1, and 2. Other parameters are $a^* = 0{\cdot}1$,

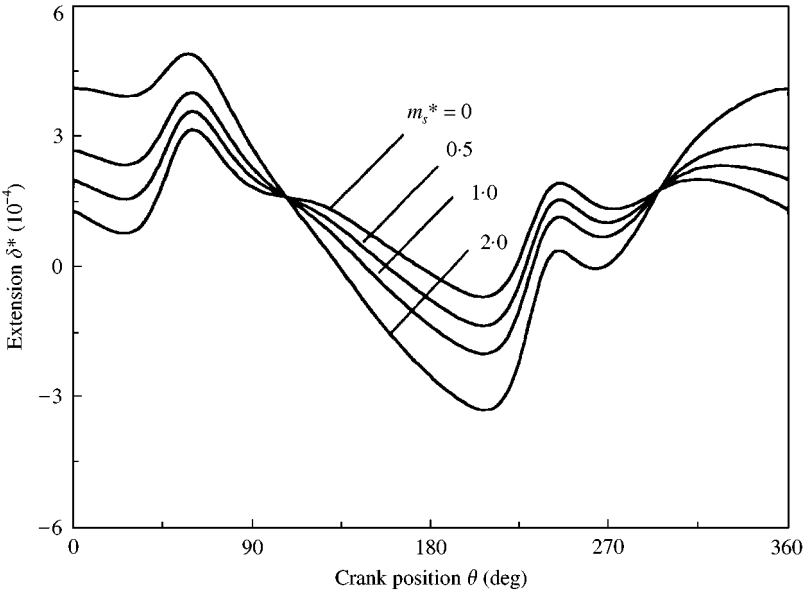

Figure 7. Extension δ^* of the connecting rod as a function of crank position θ for various values of m_s^*. $\Omega^* = 0{\cdot}8$, $\varepsilon = 0{\cdot}01$, $a^* = 0{\cdot}1$, $\mu^* = 0{\cdot}5$.

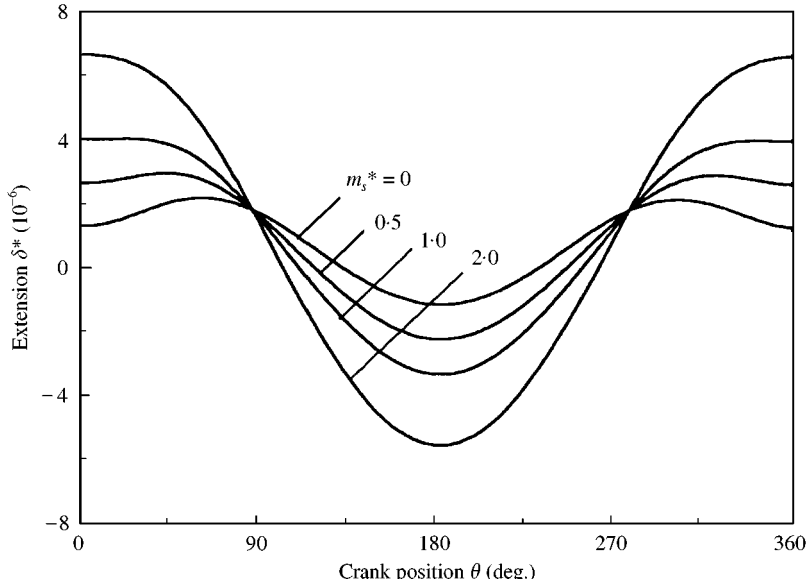

Figure 8. Extension δ^* of the connecting rod as a function of crank position θ for various values of m_s^*. $\Omega^* = 0{\cdot}1$, $\varepsilon = 0{\cdot}01$, $a^* = 0{\cdot}1$, $\mu^* = 0{\cdot}5$.

$\varepsilon = 0{\cdot}01$, and $\mu^* = 0{\cdot}5$. The dimensionless extension δ^* of the neutral axis of the connecting rod is defined and calculated as

$$\delta^* = \frac{\delta}{L} = \varepsilon^2 \int_0^1 \left[u^*_{,x^*} + \frac{1}{2}(v^*_{,x^*})^2 \right] \mathrm{d}x^*$$

$$= \varepsilon^2 u^*(1) + \frac{\varepsilon^2}{2} \int_0^1 (v^*_{,x^*})^2 \, \mathrm{d}x^*. \tag{40}$$

δ is the extension with dimension. It is interesting to note that while larger slider mass tends to induce longer extension or contraction of the neutral axis, there exist two crank positions at which the extension of the neutral axis is independent of the slider mass. These two positions are $\theta = 106{\cdot}4$ and $295{\cdot}2^\circ$ in Figure 7. A closer examination reveals that at these two positions both $u^*(1)$ and $v^*(1)$ are zero and the extension is contributed entirely from the second term of equation (40). Generally speaking, the slider position of the flexible mechanism is slightly different from the one predicted by rigid-body kinematics. However, there are two positions at which the slider position predicted by flexible mechanism theory happens to be the same as the one predicted by rigid-body kinematics. It is these two positions at which slider mass has no effect on the extension of the connection rod.

Figure 8 shows the extension for the low-speed case $\Omega^* = 0{\cdot}1$. In this case, the contribution from the second term in equation (40) is much smaller compared to the contribution from the first term. The extension diagram is almost symmetric about the position $\theta = 180^\circ$. The two positions at which extension is independent of slider mass are $\theta = 86{\cdot}4^\circ$ and 279°. At these two positions the transmission angle between the rigid crank and the connecting rod is almost 90°.

7. CONCLUSIONS

In this paper we use the finite element method to analyze the dynamic response of a slider-crank mechanism with flexible connecting rod. In the finite element formulation we retain all the high order terms in the strain-energy function. This approach results in non-linear equations of motion. The Newmark method is then adopted to calculate the transient as well as steady state responses. The effects of neglecting the high order terms in previous research studies of others are examined closely. Several conclusions can be drawn as follows:

(1) In the low-speed case $\Omega^* < 0{\cdot}2$, the non-linear approach converges as quickly as the conventional simplified approaches. Furthermore, neglecting high order terms will not produce significant errors in predicting the dynamic response.
(2) As the rotation speed increases, the non-linear approach requires more elements to achieve satisfactory convergence. More importantly, conventional approaches neglecting the high order terms begin to induce noticeable errors when $\Omega^* > 0{\cdot}2$. This error is more significant for links with small slenderness ratio.
(3) The extension and contraction of the connecting rod are much more dramatic for the high-speed case than for the low-speed one. As expected intuitively, the larger slider mass will have a more significant effect on extension. However, there exist two crank positions at which the extension of the connecting rod is independent of the slider mass.

In summary, we found that the conventional approach, neglecting high order terms in the finite element formulation for flexible mechanisms may be inadequate when the rotation speed is comparable to the fundamental natural frequencies of the flexible links. Retaining all high order terms will result in non-linear equations of motion, which certainly require more computation efforts. This is, however, a price that has to be paid in order to obtain correct results in high-speed applications.

ACKNOWLEDGMENT

The results presented here were obtained in the course of research supported by a grant (NSC89-2212-E-002-107) from the National Science Council of the Republic of China.

REFERENCES

1. A. G. ERDMAN and G. N. SANDOR 1972 *Mechanism and Machine Theory* **7**, 19–33. Kineto-elastic dynamics—a review of state of art and trends.
2. G. G. LOWEN and W. G. JANDRASITS 1972 *Mechanism and Machine Theory* **7**, 3–17. Survey of investigations into the dynamic behavior of mechanisms containing links with distributed mass and elasticity.
3. B. S. THOMPSON and C. H. SUNG 1986 *Mechanism and Machine Theory* **21**, 351–359. A survey of finite element techniques for mechanism design.
4. B. M. BAHGAT and K. D. WILLMERT 1976 *Mechanism and Machine Theory* **11**, 47–71. Finite element vibrational analysis of planar mechanisms.
5. A. MIDHA, A. G. ERDMAN and D. A. FROHRIB 1978 *Mechanism and Machine Theory* **13**, 603–618. Finite element approach to mathematical modeling of high speed elastic linkages.
6. W. SUNADA and S. DUBOWSKY 1981 *American Society of Mechanical Engineers Journal of Mechanical Design* **103**, 643–651. The application of finite element methods to the dynamic analysis of flexible spatial and co-planar linkage systems.
7. Z. YANG and J. P. SADLER 1990 *American Society of Mechanical Engineers Journal of Mechanical Design* **112**, 175–182. Large-displacement finite element analysis of flexible linkages.
8. R.-F. FUNG and H.-H. CHEN 1997 *Journal of Sound and Vibration* **199**, 237–251. Steady-state response of the flexible connecting rod of a slider-crank mechanism with time-dependent boundary condition.
9. P. K. NATH and A. GHOSH 1980 *Mechanism and Machine Theory* **15**, 179–197. Kineto-elastodynamic analysis of mechanisms by finite element method.
10. W. L. CLEGHORN, R. G. FENTON and B. TABARROK 1981 *Mechanism and Machine Theory* **16**, 407–424. Finite element analysis of high-speed flexible mechanisms.
11. D. A. TURCIC and A. MIDHA 1984 *American Society of Mechanical Engineers Journal of Dynamic Systems Measurement, and Control* **106**, 249–254. Dynamic analysis of elastic mechanism system. Part I: Applications.
12. B. S. THOMPSON and C. K. SUNG 1984 *American Society of Mechanical Engineers Journal of Mechanisms Transmissions, and Automatic Design* **106**, 482–488. A variational formulation for the nonlinear finite element analysis of flexible linkages: theory, implementation, and experimental results.
13. T. J. R. HUGHES 1986 in *Computational Methods in the Mechanics of Fracture* (S. N. Atluri, editor) Amsterdam: North-Holland. Chapter 2. Analysis of transient algorithms with particular reference to stability behavior.

APPENDIX A

We first define

$$\zeta = \frac{x}{l}.$$

The shape functions for displacements u, v, and ψ are then

$$N_{u1} = 1 - \zeta, \quad N_{u2} = \zeta, \quad N_{v1} = 1 - 3\zeta^2 + 2\zeta^3, \quad N_{v2} = \zeta(\zeta - 1)^2 l,$$

$$N_{v3} = \zeta^2(3 - 2\zeta), \quad N_{v4} = \zeta^2(\zeta - 1)l, \quad N_{\psi 1} = \frac{6\zeta}{l}(\zeta - 1),$$

$$N_{\psi 2} = 1 - 4\zeta + 3\zeta^2, \quad N_{\psi 3} = -N_{\psi 1}, \quad N_{\psi 4} = 3\zeta^2 - 2\zeta.$$

APPENDIX B

The matrices and vectors in equation (17) are

$$[\mathbf{m}_1] = \int_0^l \rho A(\{\mathbf{N}_u\}\{\mathbf{N}_u\}^{\mathrm{T}} + \{\mathbf{N}_v\}\{\mathbf{N}_v\}^{\mathrm{T}}) + \rho I(\{\mathbf{N}_\psi\}\{\mathbf{N}_\psi\}^{\mathrm{T}})\,\mathrm{d}x, \tag{B1}$$

$$[\mathbf{m}_2] = \int_0^l \rho A\,\dot{\phi}^2(\{\mathbf{N}_u\}\{\mathbf{N}_u\}^{\mathrm{T}} + \{\mathbf{N}_v\}\{\mathbf{N}_v\}^{\mathrm{T}}) + \rho I\,\dot{\phi}^2(\{\mathbf{N}_\psi\}\{\mathbf{N}_\psi\}^{\mathrm{T}})\,\mathrm{d}x, \tag{B2}$$

$$\{\mathbf{m}_3\} = \int_0^l \rho A(a\dot{\theta}\cos(\theta+\phi)\{\mathbf{N}_v\} - \dot{\phi}x_0\{\mathbf{N}_v\} - \dot{\phi}x\{\mathbf{N}_v\} - a\dot{\theta}\sin(\theta+\phi)\{\mathbf{N}_u\}) - \rho I\,\phi^2\{\mathbf{N}_\psi\}\,\mathrm{d}x, \tag{B3}$$

$$\{\mathbf{m}_4\} = \int_0^l \rho A(-a\dot{\theta}\dot{\phi}\sin(\theta+\phi)\{\mathbf{N}_v\} + \dot{\phi}^2x_0\{\mathbf{N}_u\} + \dot{\phi}^2x\{\mathbf{N}_u\} - a\dot{\theta}\dot{\phi}\cos(\theta+\phi)\{\mathbf{N}_u\})\,\mathrm{d}x, \tag{B4}$$

where x_0 is the x-co-ordinate of the ith node. The matrices in equation (18) are

$$[\mathbf{k}_{uu}] = \int_0^l EA\{\mathbf{B}_u\}\{\mathbf{B}_u\}^{\mathrm{T}}\,\mathrm{d}x, \tag{B5}$$

$$[\mathbf{k}_{\psi\psi}] = \int_0^l EI\{\mathbf{B}_\psi\}\{\mathbf{B}_\psi\}^{\mathrm{T}}\,\mathrm{d}x, \tag{B6}$$

$$[\mathbf{k}_{Pvv}] = P_i\int_0^l \{\mathbf{B}_v\}\{\mathbf{B}_v\}^{\mathrm{T}}\,\mathrm{d}x, \tag{B7}$$

$$[\mathbf{k}_{vvvv}] = \frac{1}{4}\int_0^l EA\{\mathbf{B}_{\mathrm{v}}\}\{\mathbf{B}_{\mathrm{v}}\}^{\mathrm{T}}\{\mathbf{q}\}_i\{\mathbf{B}_{\mathrm{v}}\}^{\mathrm{T}}\{\mathbf{q}\}_i\{\mathbf{B}_{\mathrm{v}}\}^{\mathrm{T}}\,\mathrm{d}x, \tag{B8}$$

where

$$P_i = EA\{\mathbf{B}_{\mathrm{u}}\}^{\mathrm{T}}\{\mathbf{q}\}_i, \tag{B9}$$

$$\{\mathbf{B}_{\mathrm{u}}\} = \frac{\mathrm{d}}{\mathrm{d}x}\{\mathbf{N}_{\mathrm{u}}\}, \tag{B10}$$

$$\{\mathbf{B}_v\} = \frac{\mathrm{d}}{\mathrm{d}x}\{\mathbf{N}_v\}, \tag{B11}$$

$$\{\mathbf{B}_\psi\} = \frac{\mathrm{d}}{\mathrm{d}x}\{\mathbf{N}_\psi\}. \tag{B12}$$

The matrices and vectors in equations (27)–(29) are defined as

$$[\mathbf{m}_{s1}] = m_s(\{\mathbf{N}_u\}\{\mathbf{N}_u\}^{\mathrm{T}} + \{\mathbf{N}_v\}\{\mathbf{N}_v\}^{\mathrm{T}})_{\zeta=1}, \tag{B13}$$

$$[\mathbf{m}_{s2}] = m_s\dot{\phi}^2(\{\mathbf{N}_u\}\{\mathbf{N}_u\}^{\mathrm{T}} + \{\mathbf{N}_v\}\{\mathbf{N}_v\}^{\mathrm{T}})_{\zeta=1}, \tag{B14}$$

$$\{\mathbf{m}_{s3}\} = m_s(-a\dot{\theta}\dot{\phi}\cos(\theta+\phi)\{\mathbf{N}_u\} - a\dot{\theta}\dot{\phi}\sin(\theta+\phi)\{\mathbf{N}_v\} + \dot{\phi}^2 L\{\mathbf{N}_u\})_{\zeta=1}, \tag{B15}$$

$$\{\mathbf{m}_{s4}\} = m_s(a\dot{\theta}\cos(\theta+\phi)\{\mathbf{N}_v\} - a\dot{\theta}\sin(\theta+\phi)\{\mathbf{N}_u\} - \dot{\phi}L\{\mathbf{N}_v\})_{\zeta=1}. \tag{B16}$$